Eur. Phys. J. B **18**, 617–624 (2000)

THE EUROPEAN PHYSICAL JOURNAL B

EDP Sciences

Evidence for the strain critical point in high T_c superconductors

D. Di Castro[1], G. Bianconi[2], M. Colapietro[3], A. Pifferi[4], N.L. Saini[5], S. Agrestini[5], and A. Bianconi[5,a]

[1] Dipartimento di Fisica, Università di Roma "La Sapienza", 00185 Roma, Italy
[2] Department of Physics, Notre Dame University, 46566 Indiana, USA
[3] Dipartimento di Chimica, Università di Roma "La Sapienza", 00185 Roma, Italy
[4] Istituto Strutturistica Chimica, Area della Ricerca, CNR, Monterotondo Stazione, Italy
[5] Unità INFM and Dipartimento di Fisica, Università di Roma "La Sapienza", 00185 Roma, Italy

Received 25 September 2000

Abstract. We report experimental evidence for the phase diagram of doped cuprate superconductors as a function of the micro-strain ε of the planar Cu-O bond length, measured by Cu K-edge EXAFS, and hole doping δ. The local lattice distortions are measured by EXAFS and the charge ordering is measured by synchrotron radiation diffuse X-ray diffraction. This phase diagram shows a QCP at $P(\varepsilon_c\delta_c)$ where for $\varepsilon > \varepsilon_c$ charge-orbital-spin stripes and free carriers co-exist. The superconducting phase occurs in the region of critical fluctuations around this QCP. The function $T_c(\varepsilon, \delta)$ of two variables shows its maximum at the strain QCP. The critical fluctuations near this strain QCP give the self-organization of a metallic superlattice of quantum wires "superstripes" that favors the amplification of the critical temperature.

PACS. 74.72.-h High-T_c compounds – 61.10.-i X-ray diffraction and scattering – 78.70.Dm X-ray absorption spectra

1 Introduction

The normal phase of the cuprate perovskites has been considered to depend on a single variable: the charge density measured by the doping δ, *i.e.*, the distance from the charge density of one hole for Cu site giving the Mott Hubbard antiferromagnetic phase. The phase diagram of cuprates remains mysterious after 13 years of extensive research [1]. Experiments have shown characteristic features of a non Fermi liquid behavior in transport properties and anomalous spin [2] and lattice fluctuations [3] typical of the proximity to a quantum critical point (QCP) [4]. Several types of quantum phase transitions (QPT) as a function of doping have been proposed [5–9] without success since it has not been possible to identify the location of the QCP at a critical doping. The QPT is a zero temperature generically continuous transition tuned by a parameter in the Hamiltonian where quantum fluctuations take the system between two distinct ground states. The fluctuations between two nearly degenerate ground states is the characteristic feature of complex systems such as biological molecules [10]. Self organization is expected near a QCP and the striped phases [11,12] observed in some cuprate perovskites is a manifestation that the ground state fluctuates between two states. In fact the striped phases appear where the system fluctuates between two states and the one-dimensional long range ordering is driven by a long range elastic, Coulomb or magnetic field. Recently it has been shown that the phase diagram of cuprate perovskites can be resolved by introducing a new axis: the elastic strain field on the CuO_2 plane [12,13]. In fact, the local micro-strain of the Cu-O bonds ε is the second variable needed to define the metallic phase of doped cuprates. The quantum critical point QCP, driving the quantum fluctuations relevant for the superconducting pairing, is not on the axis of doping at zero micro-strain but at the point $(P_c(\delta_c, \varepsilon_c))$ at finite micro-strain. We show here that both local lattice distortions and 1D charge and orbital ordering appear for a micro-strain larger than the critical value $\varepsilon > \varepsilon_c$, therefore the micro-strain QCP is the critical point for stripes formation. The 2D plot $(T_c(\delta, \varepsilon)$ shows that the highest $T_c \sim 150$ K occurs at this QCP. The cuprate perovskites are heterogeneous materials [14] made of three different portions: first, metallic bcc CuO_2 layers, (second) insulating rock-salt fcc AO_{1-x} layers (A = Ba, Sr, La, Nd, Ca, Y...) and (third) charge reservoir (CR) BO_{1-x} layers. The superconducting covalent bcc CuO_2 layer is intercalated between insulating fcc ionic rock-salt AO layers, rotated by 45°. The mismatch between the two sub-lattices is $\eta = 1 - t = [R(\text{A-O})/\sqrt{2}[R(\text{Cu-O})]$ where R(A-O) is the sum of the average metal ion radius in the rock-salt layer r_A and the O^{2-} radius, R(Cu-O) is the Cu-O bond length and t is called the Goldschmidt tolerance factor. It is known that in hole doped superconducting cuprates, the CuO_2 sheets are under compression due to the lattice mismatch. Several experiments have shown

[a] e-mail: bianconi@superstripes.com

that the mismatch between the two sub-lattices have a significant effect on the superconducting transition temperature [15–19]. A large shear compressive stress is exerted on the CuO_2 plane by the lattice mismatch with the rocksalt layers with a strong adhesive force from the substrate. Following the classical theory of elasticity a uniform strain of the CuO_2 plane is expected for a small misfit and above a critical misfit η^* and there are two possibilities [20]: The first possibility is discommensuration, that is a narrow region where the atoms of a bcc layer, embedded between two fcc layers, are out of registry with the minima of the substrate induced periodic potential. The misfit is absorbed by a periodic array of discommensurations which separate the regions of commensurate registry. A second possibility is pseudomorphism where the bcc layer adopts a crystal structure that is well matched to the fcc substrate but differs from the crystal structure that the compound will adopt in the bulk. At a critical value of the misfit η^* the coherent-incoherent transition is triggered by an instability toward a modulated spinodal structure with a wave-vector q of a strain wave spinodal decomposition. A martensitic transition could occur to an incoherent metastable structure characterized by a macroscopic domain structure that contains periodic arrays of twin and slip boundaries. The striped phase made of 1D incommensurate modulation with alternated stripes of LTT and LTO local CuO_2 lattice observed in Bi2212 and La124 systems remind a type of spinodal decomposition of two pseudomorphic phases of CuO_2 lattice, where two types of cooperative tilting are alternated forming an incommensurate superlattice of mesososcopic stripes [21,22]. The metallic phase in the CuO_2 plane is obtained by two separate steps: *first*, the doping δ in the CuO_2 plane is controlled by introducing the chemical dopants in the block layers. In clean systems the dopants are introduced in the charge reservoir layers, far from the metallic CuO_2 plane. In dirty systems the dopants enters the rocksalt AO layers forming impurity centers that give a disordered metallic phase in the CuO_2 plane, as is the case of Sr doped La_2CuO_4. *Second*, the compressive stress on the CuO_2 plane is controlled by multiple substitutions of metal ions A (A = Ba, Sr, La, Nd, Ca, Y...) in the oxygen deficient rock-salt (AO) layers. In fact, we found that the microstrain of the average Cu-O bond depends on the average ionic radius $\langle r_A \rangle$ of the rock-salt layers but not on the dopants in the charge reservoir (BO) blocks. There are now a growing number of experiments providing evidence for electron lattice interaction being a necessary parameter to characterize the metallic state of the cuprates [23–29]. Recent experiments on the isotope effects [30–32] have further stressed the need to include the electron lattice interaction as one of the parameters to describe the complex metallic phase of the cuprate superconductors. The compressive stress induces an elastic strain field ε in the CuO_2 plane that changes the electron-lattice interaction $g(\varepsilon)$. For example, the pseudo Jahn-Teller (JT) electron-phonon coupling [24,25], $g_{JT} = \Psi(Q, \Delta_{JT}, \beta)$, depends on the conformational parameter for the local distortions of the CuO_4 square Q as the rhombic distortion of CuO_4 square plane, the dimpling angle β given by the displacement of the Cu ion from the plane of oxygen ions, and the Cu-O (apical) bond length that controls JT energy splitting Δ_{JT}. Therefore by changing the strain field the system can be driven towards the critical point for charge localization where localized and delocalized charges can co-exist. The complex physics of cuprates is due to the fact that the metallic phase is made by doping, δ, that shifts the system away from the Mott-Hubbard insulating phase. The doped charges are expelled from the antiferromagnetic domains and an inhomogeneous metallic phase is formed as for doped magnetic insulators [33]. Therefore the phase of the metallic state in these systems is determined by both the doping (that changes the ratio t/J) and the micro-strain (that changes the electron lattice interaction g). At low doping in the weak electron lattice (e-l) interaction a glassy phase of charge stripes in the antiferromagnetic background is expected. At large (e-l) interaction we expect the formation of strings of charges trapped in local lattice distortions, in an antiferromagnetic background. At an intermediate (e-l) coupling and higher doping a complex phase appears with the coexistence of free carriers and stripes, where carriers are trapped in the cooperative local lattice distortion [35,36]. Therefore the phase diagram of the cuprates requires a second axis the micro-strain ε at the Cu site [13] beyond doping. We have measured the micro-strain at the Cu site by exploiting the Cu K-edge extended X-ray absorption fine structure (EXAFS) that is a local and fast structural probe. From the average $\langle R_{Cu\text{-}O} \rangle$ in the CuO_2 plane we have measured the micro-strain of the Cu-O bond defined as $\varepsilon = 2\frac{d_0 - \langle R_{Cu\text{-}O} \rangle}{d_0}$ where the factor 2 is introduced to get the ratio $\varepsilon/\eta \sim 1$. Here d_0 is Cu-O equilibrium distance, *i.e.*, Cu-O bond length for an unstrained CuO_2 plane, $d_0 \sim 1.985(\pm 0.005)$ Å on an undoped model system $Sr_2CuO_2Cl_2$, which is consistent with others [37]. d_0 is taken to be 1.97 Å throughout this paper considering the effect of Cu-O shortening at optimum doping ($\delta \sim 0.16$ doped holes per Cu site). To avoid the disorder created by cationic substitution we have selected the clean superconducting systems where the doping is provided only by the interstitial oxygen in the charge reservoir blocks. We have measured the temperature dependence of local lattice distortions *via* the Cu-O pair distribution function and charge ordering by X-ray scattering. The results provide a direct experimental evidence for stripe formation above a critical micro-strain and the superconducting transition temperature reaches the maximum at the micro-strain quantum critical point (QCP).

2 Experimental

Well-characterized single layer superconducting single crystals of different superconducting systems were used for the experiments. The $La_2CuO_{4.1}$ (LCO), $HgBa_2CuO_{4+\delta}$ (Hg1201) systems are used as representative for the [BO](AO)CuO_2 heterostructures: $[O_\delta](La_2O_2)CuO_2$, and $[HgO_\delta](Ba_2O_2)CuO_2$, where the (AO) rock-salt layers sustain different strain on the CuO_2 planes, and the dopants

are interstitial oxygen ions in the charge reservoir layers [BO]. The data are compared with previous results on two layer compounds Bi2212, $[Bi_2O_{2+\delta}](Sr_2O_2Ca)Cu_2O_4$, and Hg1212 $[HgO_\delta](Ba_2O_2)CuO_2$.

An electrochemically doped LCO single crystal of size 2×2 mm^2 was used [38,39]. This crystal has been characterized by X-ray diffraction showing 3.5 staging and single $T_c \sim 40$ K ($\Delta T_c \sim 1.5$ K) measured before the experiments. The oxygen ordering of stage 3.5 occurs between 330 K to 270 K.

The Hg-based crystals were of small size ($\sim 0.3 \times 0.3$ mm^2), and were grown by high-pressure synthesis technique [40]. The T_c of the samples used for the present experiments were 94 K ($\Delta T_c \sim 2$ K) for the Hg1201.

The temperature dependent polarized Cu K-edge absorption measurements were performed on the beam-lines BM29 and BM32 of European Synchrotron Radiation Facility (ESRF), Grenoble. The crystals were mounted in a closed cycle refrigerator and temperature was controlled to within an accuracy of ± 1 K. Beam-line BM29 of ESRF is equipped with a two stage closed cycle refrigerator. In all cases, the temperature was measured using diode sensors attached to the flat plate sample holder. The measurements were performed in the fluorescence yield (FY) mode [42] using multi-element Ge X-ray detectors array. The emphasis was given to measure the spectra with a high signal to noise ratio and up to a high momentum transfer and purposefully we measured several scans to accumulate the total fluorescence counts to be ~ 3 millions to limit the relative errors to be less than 0.1% above the absorption threshold. Standard procedure was used to extract the EXAFS signal from the absorption spectrum and corrected for the X-ray fluorescence self-absorption before the analysis [41,42].

The charge ordering has been studied by temperature dependent diffraction data collected on the crystallography beam-line at the synchrotron radiation facility Elettra at Trieste. The X-ray beam emitted by the wiggler source on the 2 GeV electron storage ring was monochromatized by a Si(111) double crystal monochromator, and focused on the sample. The temperature of the crystal was monitored with an accuracy of ± 1 K. We have collected the data with a photon energy of 12.4 KeV, wavelength $\lambda = 1$ Å, using an imaging plate as a 2D detector. The sample oscillation around the **b** axis was in a range $0 < \phi < 30°$, where ϕ is the angle between the direction of the photon beam and the **a** axis. We have investigated a portion of the reciprocal space up to 0.6 Å^{-1} momentum transfer, *i.e.*, recording the diffraction spots up to the maximum indices 3, 3 and 19 in the $\mathbf{a}^*$, $\mathbf{b}^*$ and $\mathbf{c}^*$ direction respectively.

3 Results and discussion

Figure 1 shows the EXAFS signals extracted from the Cu K-edge absorption spectra measured on two different superconducting systems with $\mathbf{E} \parallel \mathbf{ab}$ plane (multiplied by k^2 to emphasize the higher k-region). The EXAFS oscillations are clearly visible up to the high k-values required

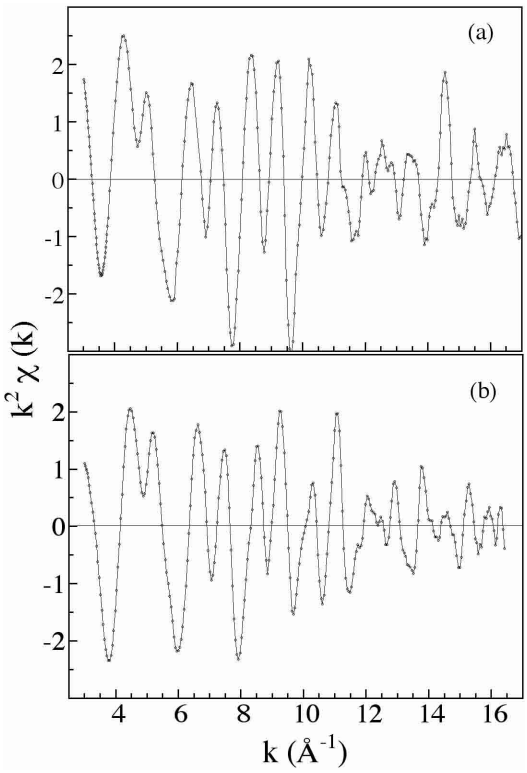

Fig. 1. Cu K-edge EXAFS spectra on the representative systems measured in their superconducting state; $La_2CuO_{4.1}$ (LCO, upper panel) and Hg1201 (lower panel). The EXAFS signal was extracted from the absorption spectra measured on single crystal samples using multi-element fluorescence detector systems in the $\mathbf{E} \parallel \mathbf{ab}$ geometry. The emphasis is given to obtain the spectra with high signal-to-noise ratio and the EXAFS oscillations up to high k-value.

to solve quantitative local distortions in these complex systems. The EXAFS [43] oscillations are due to backscattering of photoelectrons, emitted at the Cu site, from neighboring atoms providing a global atomic distribution around the absorbing Cu site.

Here we focus only on the local distortions in the CuO_2 plane and hence the first oxygen coordination shell (*i.e.* in-plane Cu-O bond distances). In the $\mathbf{E} \parallel \mathbf{ab}$ Cu K- edge EXAFS the signal due to the Cu-O bond distances is well separated from the longer bond contributions and can be easily extracted and analyzed separately. The extracted EXAFS signals due to the Cu-O bond distances represent only single backscattering of the photoelectron emitted at the Cu site by its nearest neighbor in-plane oxygen atoms and thus probe the correlation function of the Cu-O pairs. The approach is to avoid any multiple scattering signals that generally make the data analysis complex. We have used the standard procedures to draw the pair distribution function (PDF) of local Cu-O bond-lengths from analysis of the EXAFS oscillations only due to the Cu-O distances. In this procedure the EXAFS signal due to the Cu-O is simulated by standard least squares fit with an input of a distribution distances (where the $N_{\rm tot}$ is fixed to the nominal value and $\sigma^2_{\rm CuO}$ for each distance

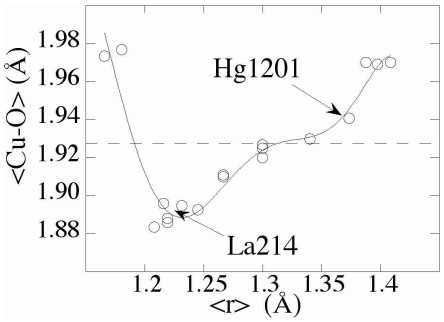

Fig. 2. The average $\langle R_{\text{Cu-O}} \rangle$ bond length measured by Cu K-edge EXAFS as a function of the average radius $\langle r_{\text{A}} \rangle$ of metal ions in the rocksalt layers for all cuprate perovskites. From these data the micro-strain, $\varepsilon = 2\frac{d_0 - \langle R_{\text{Cu-O}} \rangle}{d_0}$ with $d_0 = 1.97$ Å is measured.

to the values given by Einstein model for correlated Cu-O distribution) respecting the number of allowed parameter to be less than $(2\Delta R \Delta k/\pi)$ [43]. The feasibility of these methods has been shown in the case of cuprates [22,42] and manganites [44] and other complex systems [45,46].

We report in Figure 2 the variation of the average local $\langle R_{\text{Cu-O}} \rangle$ distance as measured herein as well as those measured earlier. From the measure of $\langle R_{\text{Cu-O}} \rangle$ we can obtain the direct measure of the value of the local micro-strain on the Cu-O bond $\varepsilon = 2\frac{d_0 - \langle R_{\text{Cu-O}} \rangle}{d_0}$ (where $d_0 = 1.97$ Å) in the various cuprate perovskites. The Cu-O bond length shows a decrease, indicating an increasing compressive strain of the Cu-O bond, with decreasing of the average ionic radius in the rocksalt layers. The structure remains stable until the value of the strain reaches where the CuO_2 plane, or the rocksalt layer or both relax to a different structure that corresponds to a pressure of about 25 GPa [19]. The two samples La214 and Hg1201 studied here respectively lie below and above the horizontal dashed line indicating the critical micro-strain for stripe formation.

In Figure 3 we report the PDF of our crystals with different micro-strain as a function of temperature. The PDF of Hg1201 shows the typical temperature dependence of systems where $\varepsilon < \varepsilon_{\text{c}}$, $\varepsilon_{\text{c}} = 4.5\%$. A very broad PDF appears but no splitting of the Cu-O distance. We observe that, in $La_2CuO_{4.1}$ where the micro-strain is larger than the critical micro-strain $\varepsilon_{\text{c}} \sim 0.045$ the PDF shows the onset of local lattice distortions identified by the presence of two peaks in the PDF at $T < T_{\text{co}}$. We have determined the critical temperature for the formation of the local lattice distortion $T_{\text{co}} = 190$ K by measuring the onset of the deviation from the Gaussian distribution and splitting of the PDF as shown in Figure 4.

The temperature T_{co} for the onset of local lattice distortions should be compared with $T_{\text{co}} = 120$ K in Bi2212 where $\varepsilon > \varepsilon_{\text{c}}$ [21,41]. In Bi2212 it has been observed that the coupling of electrons with dynamical charge fluctuations with wave-vector $q_{\text{cdw}} = 0.4\pi, 0.4\pi$ induces a suppression of the spectral weight near the M point also above the stripe formation temperature indicating dynamical fluctuations near a critical point [47]. Moreover, the

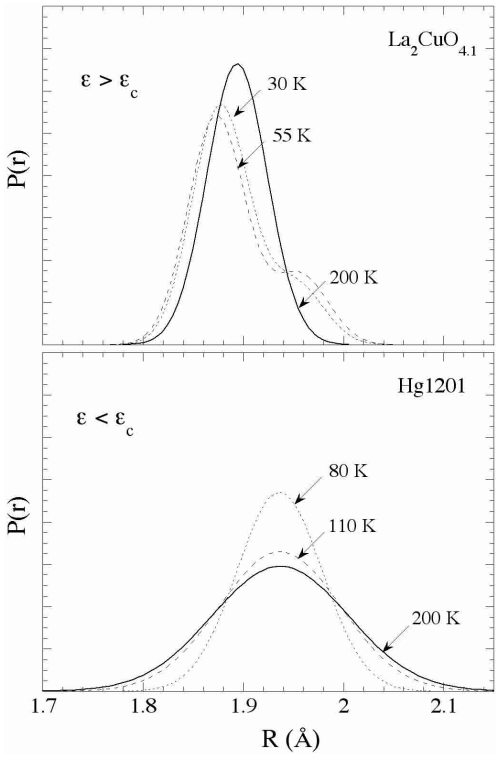

Fig. 3. Cu-O pair distribution function (PDF) as a function of temperature for the two different systems above and below the critical micro-strain. The PDF of Hg1201 shows the typical temperature dependence of systems where $\varepsilon < \varepsilon_{\text{c}}$, $\varepsilon_{\text{c}} = 4.5\%$. A very broad PDF appears but not any splitting of the Cu-O distance. The PDF of $La_2CuO_{4.1}$ (LCO) shows the typical behavior of systems where $\varepsilon > \varepsilon_{\text{c}}$. Evidence for local lattice distortions is indicated by the deviation from a Gaussian distribution and two peaks below a temperature T_{co}.

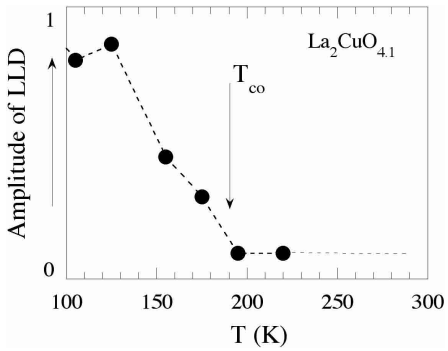

Fig. 4. The temperature dependence of the onset of local lattice distortions measured by the deviation from the single Gaussian PDF and appearance of an anomalous long bond.

particular wave-vector is such that the density of states at the Fermi level is enhanced and not suppressed by the onset of stripe formation as expected for dynamical self-organization of the superlattice of quantum stripes at a shape resonance [48].

We have investigated the charge ordering in LCO, by that remains orthorhombic in the superconducting phase, by X-ray diffraction. A large number of weak

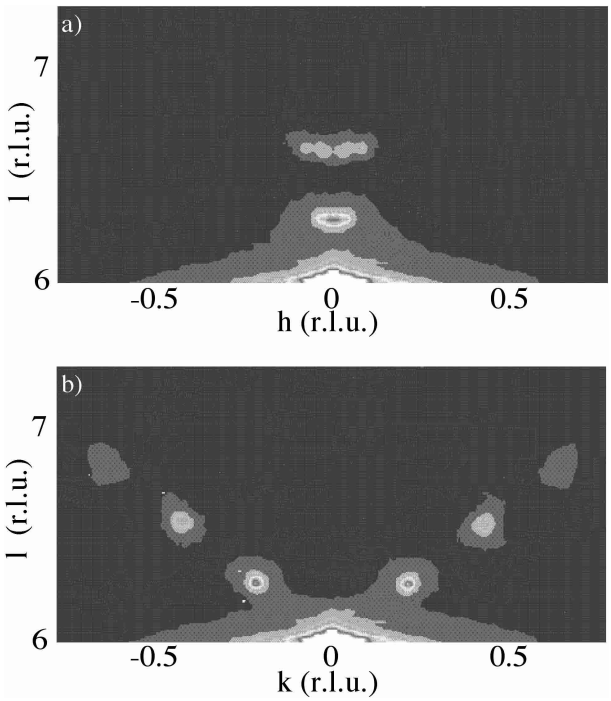

Fig. 5. The X-ray diffraction pattern detected by the imaging plate of the diffuse peaks of stage 3.5 superstructure in superconducting $La_2CuO_{4.1}$ near the 006 main diffraction spot. The peaks due to the $\mathbf{a}^*\mathbf{c}^*$ reciprocal lattice are shown in panel (a). The peaks due to the $\mathbf{b}^*\mathbf{c}^*$ reciprocal lattice are shown in panel (b).

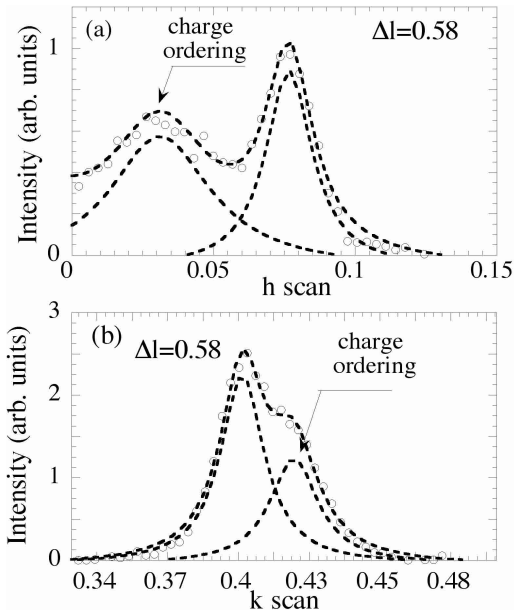

Fig. 6. Scans along the $Q = (h, 0, 6 + \Delta l)$ (panel (a)) and along the $Q = (0, k, 6 + \Delta l)$ (panel (b)) due to the scattering peaks of stage 3.5 superstructure. The charge ordering diffuse peak and the oxygen ordering peaks can be resolved.

superstructure spots due to stripe formation around the main peaks of the average structure have been measured. The indexing of the superstructure has been conducted taking into account the twinning of the crystal. The oxygen ordering has been found to occur in the temperature range 270–330 K. The metallic superconducting phase of our crystal shows an X-ray diffraction pattern due to the modulation around the main (0,0,6) spot in the $\mathbf{a}^*$ and $\mathbf{b}^*$ directions as shown in Figure 5. The profile of the peaks of the second harmonic is shown in Figure 6. We have been able to separate the modulation due to the 3D oxygen ordering from stripe formation. In fact, in Figure 6, it is possible to distinguish the narrow peaks due to the oxygen ordering and with a finite $\mathbf{a}^*$ component, from the peaks due to superstripes [48] that are diffuse indicating the stripes formation in bubbles of finite size. The incommensurate modulation is indicated by a pattern of diffuse charge ordering spots with coherence length of about 350 Å and with wave-vector: $\mathbf{q}_{\rm cdw} = 0.0126(\pm 0.0003)\,\mathbf{a}*,\ 0.2080(\pm 0.003)\,\mathbf{b}*,\ 0.290(\pm 0.005)\,\mathbf{c}*$, and a commensurate in-plane modulation with a pattern of narrower diffraction spots, due to the oxygen ordering, with wave-vector: $\mathbf{q}_{\rm oxy} = 0.037(\pm 0.001)\,\mathbf{a}*,\ 0.198(\pm 0.002)\,\mathbf{b}*,\ 0.290(\pm 0.005)\,\mathbf{c}*$.

Along the $\mathbf{b}^*$ direction (Fig. 5) the third harmonic of the $\mathbf{q}_2$ modulation is also observed, showing the evidence of the anharmonicity of this modulation. The length of the stripes in the $\mathbf{a}^*$ direction becomes larger than $57a$ (~ 300 Å) of the same order of magnitude as the coherence length of the modulation. Therefore the superconducting stripes appear in bubbles of 300 Å diameter.

The profiles of the second harmonic peaks of this domain along the $\mathbf{b}^*$ and $\mathbf{a}^*$ directions are shown in the panels (a) and (b) of Figure 6 respectively. In this figure we can clearly separate, both in the $\mathbf{b}^*$ and $\mathbf{a}^*$ directions, the oxygen modulation, with long coherence length $1/\Gamma = 101.5a$ (with $\Gamma = 0.009855$), from the charge modulation, with short coherence length $1/\Gamma = 44.5a$ (with $\Gamma = 0.02248$). The two curves fitted to the experiment are also shown (dashed lines). We have studied the temperature dependence from room temperature to 100 K of the charge ordering indicated by the diffuse peaks in the second harmonic that can be separated from the oxygen ordering peaks. The square root of the intensity of the diffraction lines, plotted in Figure 6, gives a direct measure of the density of charge $\Delta\rho(q)$ that gets ordered in the CuO_2 plane with wave-vector q, that is the order parameter for the charge ordered phase. The temperature dependence is shown in Figure 7 and the solid line is a fit to the experimental intensities with an expression $\Delta\rho \propto (T - T_{\rm co})^{\alpha}$ with $T_{\rm co} \sim 190$ K. This effect is clearly due to formation of charge stripes in the CuO_2 plane since the oxygen mobility is frozen below 250 K. In fact, the 3D oxygen ordering has already been established at higher temperature (at $\sim$270–230 K) in the system as evidenced by temperature evolution of the resolution-limited diffraction peaks. This result shows that the $T_{\rm co}$ is the stripe formation temperature since it is the onset of both charge ordering, shown in Figure 7, and local lattice distortions, shown in Figure 4.

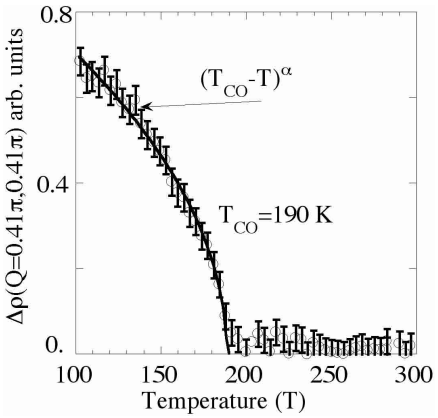

Fig. 7. Temperature dependence of the order parameter for the charge ordering (the square root of the intensity of the diffuse peak due to stripe formation) with wave-vector $q(0.4\pi, 0.4\pi)$ in $La_2CuO_{4.1}$. The fit shows a critical temperature $T_{co} = 190$ K for charge ordering.

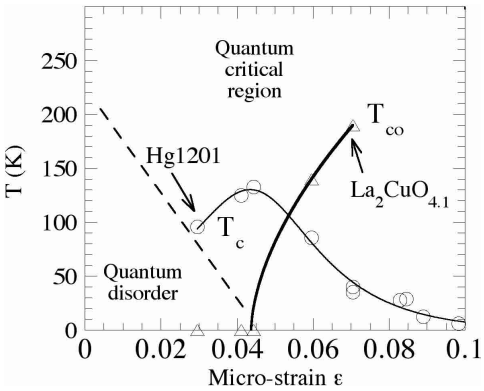

Fig. 8. The critical temperature for stripe formation T_{co} and the superconducting critical temperature T_c as function of the micro-strain $\varepsilon = 2\frac{d_0 - \langle R_{Cu\text{-}O} \rangle}{d_0}$ at optimum doping $\delta = 0.16$.

The second harmonic indicates a transverse modulation of the superlattice of stripes in plane along the **b**-axis with a wave-vector of 0.416**b*** indicating a separation between the stripes of ~ 2.5**b** along the **b** axis. The period of the superlattice is 3.5**c** along the **c** axis.

We plot in Figure 8 the value of the temperature for the onset of local lattice distortions and the 1D ordering of localized charge as a function of the micro-strain ε for different samples. It is clear that the micro-strain ε drives the system to a quantum critical point for the formation of a superlattice of quantum stripes for $\varepsilon > \varepsilon_c \sim 4.5\%$. In the same figure we report the critical temperature T_c that shows a maximum at the critical micro-strain.

In Figure 9 we report a color plot (the critical temperature increases from black, $T_c = 0$ K, to white, the maximum $T_c \sim 135$ K) as a function of the micro-strain ε and doping δ for all main superconducting cuprate families. The figure shows that the maximum T_c occurs at the critical point $P_c = (\delta_c = 0.16 \pm 0.04 \varepsilon_c = 0.045 \pm 0.005)$.

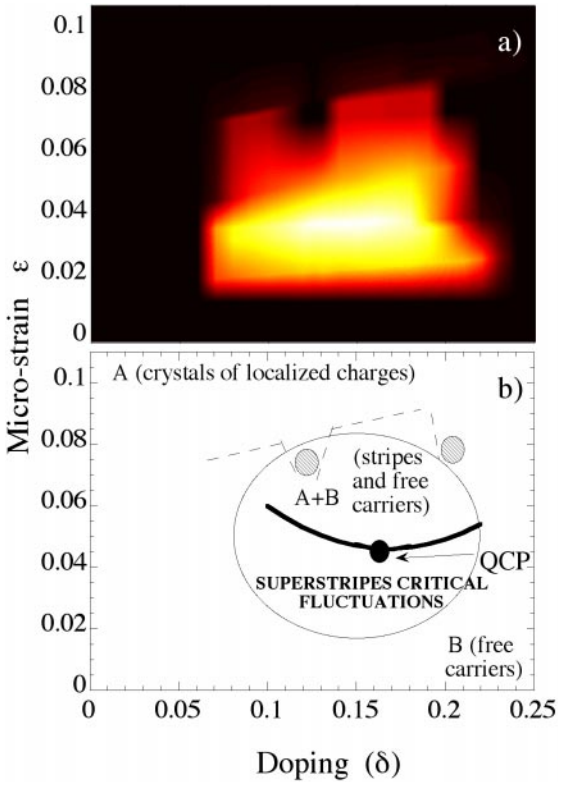

Fig. 9. Panel (a): the superconducting critical temperature T_c plotted in a hot metal color scale (from $T_c = 0$ K, black, to $T_c \sim 135$ K, white) as a function of the micro-strain ε and doping δ. The maximum T_c occurs at the critical point $\delta_c = 0.16 \pm 0.3$, and $\varepsilon_c = 0.045 \pm 0.01$. Panel (b): the phase diagram for the normal phase of doped cuprate perovskites as a function of micro-strain and doping. with the region of quantum fluctuations around the micro-strain quantum critical point QCP.

From these data we can derive the phase diagram for the cuprate perovskites shown in panel (b) of Figure 9. This phase diagram may solve the long standing puzzle of the phase diagram of the normal phase of the cuprates. The micro-strain triggers the electron-lattice interaction at a critical value g^* for the onset of charges trapped into a striped phase with dynamical and spatial ordering of pseudo Jahn Teller local lattice distortions (JT-LLD) over mesoscopic bubbles of 100–300 Å. The doping of the strained antiferromagnetic lattice forms both free carriers and charges trapped into the JT- LLD above the critical micro-strain ε_c. For $\varepsilon > \varepsilon_c$, as it was discussed for the case of oxygen doped Bi2212 and La214, the systems show a quasi first order phase transition as a function of doping [21]. The quantum critical point QCP is well identified in the curve at constant doping as a function of the micro-strain ε, shown in Figure 8.

In conclusion, we have shown that above the critical micro-strain in oxygen doped La_2CuO_4 the temperature for the onset of local lattice distortion and stripe formation is $T_{co} = 190$ K. We have deduced a phase diagram

for the superconducting phases where T_c depends on both doping and micro-strain. The anomalous normal phase of cuprate superconductors is determined by inhomogeneous phases with co-existing stripes and itinerant carriers that appears above a critical micro-strain of the Cu-O bonds. This experiment shows a strong interplay of fluctuations of orbital, charge and spin stripes in this critical regime. The micro-strain drives the electron lattice interaction to a QCP of a quantum phase transition where the stripes get self organized in a superlattice of quantum wires into mesoscopic bubbles of about 300 Å size. In this inhomogeneous phase charges trapped into JT-LLD co-exist with free carriers and the chemical potential is tuned to a shape resonance [48].

This research has been supported by the Ministero dell'Università e della Ricerca Scientifica (MURST) under the Programmi di Ricerca Scientifica di Rilevante Interesse Nazionale, by Istituto Nazionale di Fisica della Materia (INFM) and by Progetto 5% Superconduttività del Consiglio Nazionale delle Ricerche (CNR).

References

1. B. Batlogg, C.M. Varma, Phys. World **13**, 33 (2000).
2. G. Aeppli, T.E. Manson, S.M. Hayden, H.A. Mook, J. Kulda, Science **278**, 1432 (1997).
3. R.P. Sharma, S.B. Ogale, Z.H. Zhang, J.R. Liu, W.K. Chu, B. Veal, A. Pauliskas, H. Zheng, T. Venkatesan, Nature **404**, 736 (2000).
4. S. Sachdev, *Quantum Phase Transitions* (Cambridge Univ. Press, New York, 1999).
5. A.J. Millis, S. Sachdev, C.M. Varma, Phys. Rev. B **37**, 4975 (1988).
6. A.J. Millis, H. Monien, D. Pines, Phys. Rev. B **42**, 167 (1990).
7. N.E. Bikers, S.R. White, Phys. Rev. B **43**, 8044 (1991).
8. R. Micnas, S. Robasziewicz, Phys. Rev. B **45**, 9900 (1992); *ibid.* Phys. Rev. B **52**, 6863 (1995); R. Micnas, S. Robaszkiewicz in, *High T_c Superconductivity: Ten years after the Discovery* (Nato ASI, Vol. 343), edited by E. Kaldis, E. Liarokapis, K.A. Müller (Dordrecht, Kluwer, 1996) p. 31.
9. A. Perali, C. Castellani, C. Di Castro, M. Grilli, Phys. Rev. B **54**, 16216 (1996).
10. H. Frauenfelder S.G. Sligar, P.G. Wolynes, Science **254**, 1598 (1991).
11. A. Bianconi, in *Phase Separation in Cuprate Superconductors*, edited by K.A. Muller, G. Benedek (World Scientific Singapore, 1993) p. 352; *ibidem* p. 125; A. Bianconi, M. Missori, J. Phys. I France **4**, 361 (1994).
12. A. Bianconi, S. Agrestini, G. Bianconi, D. Di Castro, N.L. Saini, in *Stripes & Related Phenomena*, edited by A. Bianconi, N.L. Saini (Klüwer/Plenum publishers, New York) p. 9 (2000); see the web site `http://www.superstripes.com/`
13. A. Bianconi, G. Bianconi, C. Caprara, D. Di Castro, H. Oyanagi, N.L. Saini, J. Phys. Cond. Matt. **12**, 10655 (2000).
14. J.B. Goodenough, Supercond. Science Techn. **3**, 26 (1990); J.B. Goodenough, A. Marthiram, J. Sol. State Chem. **88**, 115 (1990); C.N.R. Rao, A.K. Ganguli, Chem. Soc. Rev. **24**, 1 (1995).
15. J.P. Attfield, A.L. Kharlanov, J.A. McAllister, Nature **394**, 157 (1998).
16. J.P. Locquet, J. Perret, J. Fompeyrine, E. Mächler, J.W. Seo, G. Van Tendelloo, Nature **394**, 453 (1998).
17. H. Ihara, Bulletin of Electrotechnical Lab., **58**, 64 (1994); also see *e.g.* F. Izumi, E. Takayama-Muromachi, in *High Temperature Superconducting Materials and Engineering*, edited by D. Shi (Pergamon, 1995) p. 81.
18. H. Sato, A. Tsukada, M. Naito, A. Matsuda, Phys. Rev. B **61**, 12447 (2000).
19. M. Marezio, F. Licci, Physica C **282**, 53 (1997).
20. A. Bruinsma, A. Zangwill, J. Phys. France **47**, 2055 (1986).
21. A. Bianconi, Sol. State Commun. **91**, 1 (1994); A. Bianconi, Physica C **235-240**, 269 (1994).
22. A. Bianconi, N.L. Saini, A. Lanzara, M. Missori, T. Rossetti, H. Oyanagi, H. Yamaguchi, K. Oka, T. Ito, Phys. Rev. Lett. **76**, 3412 (1996).
23. J.G. Bednorz, K.A. Müller, Z. Phys. B **64**, 189 (1986); J.G. Bednorz, K.A. Müller, Rev. Mod. Phys. **60**, 565 (1988).
24. Y. Seino, A. Kotani, A. Bianconi, J. Phys. Soc. Jpn **59**, 815 (1990).
25. G.I. Bersuker, J.B. Goodenough, Physica C **274**, 267 (1997); J.-S. Zhou, J.B. Goodenough, Phys. Rev. B **56**, 6288 (1997).
26. K.A. Müller, Guo-meng Zhao, K. Conder, H. Keller, J. Phys. Cond. Matt. **10**, L291 (1998).
27. E.S. Bozin, S.J.L. Billinge, G.H. Kwei, H. Takagi, Phys. Rev. B **59**, 4445 (1999).
28. R.J. McQueeney, Y. Petrov, T. Egami, M. Yethiraj, G. Shirane, Y. Endoh, Phys. Rev. Lett. **82**, 628 (1999).
29. N.L. Saini, A. Lanzara, A. Bianconi, H. Oyanagi, Eur. Phys. J. B **18**, 257 (2000).
30. A. Lanzara, G.-m. Zhao, N.L. Saini, A. Bianconi, K. Conder, H. Keller, K.A. Müller, J. Phys. Cond. Matt. **11**, L541 (1999).
31. D. Rubio Temprano, J. Mesot, S. Janssen, K. Conder, A. Furrer, H. Mutka, K.A. Müller, Phys. Rev. Lett. **84**, 1990 (2000).
32. J. Hofer, K. Conder, T. Sasagawa, Guo-meng Zhao, M. Willemin, H. Keller, K. Kishio, Phys. Rev. Lett. **84**, 4192 (2000) and references therein.
33. E.L. Nagaev Sov. Jour. JEPT Lett. **16**, 558 (1972); V.A. Kaschin, E.L. Nagaev, Zh. Exp. Teor. Phys. **66**, 2105 (1974); E.L. Nagaev, A.I. Podelshchikov, V.E. Zil'berwarg J. Phys. Cond. Matt. **10**, 9823 (1998); E.L. Nagaev, *Physics of Magnetic Semiconductors* (Mir Publisher, Moscow, 1983).
34. F.V. Kusmartsev J. Phys. IV France **9**, Pr10-321 (1999); F.V. Kusmartsev, Phys. Rev. Lett. **84**, 530 (2000); *ibidem* **84**, 5026 (2000).
35. V. Cataudella, G. De Filippis, G. Iadonisi, Phys. Rev. B **60**, 15163 (1999); V. Cataudella, G. De Filippis, G. Iadonisi, A. Bianconi, N.L. Saini, J. Mod. Phys. (2000) to be published.

36. F.V. Kusmartsev, D. Di Castro, G. Bianconi, A. Bianconi, Phys. Lett. A **275**, 118 (2000).
37. L.L. Miller, X.L. Wang, S.X. Wang, C. Stassis, D.C. Johnston, J. Faber, Jr, C.-K. Loong, Phys. Rev. B **41**, 1921 (1990).
38. F.C. Chou, D.C. Johnston, S.W. Cheong, P.C. Canfield, Physica C **216**, 66 (1993).
39. A. Bianconi, D. Di Castro, G. Bianconi, A. Pifferi, N.L. Saini, F.C. Chou, D.C. Johnston, M. Colapietro, Physica C **341-348**, 1719 (2000).
40. J. Karpinski, H. Schwer, I. Mangelschots, K. Conder, A. Morawski, T. Lada, A. Paszewin, Physica C **234**, 10 (1994).
41. N.L. Saini, A. Lanzara, H. Oyanagi, H. Yamaguchi, K. Oka, T. Ito, A. Bianconi, Phys. Rev. B **55**, 12759 (1997); A. Lanzara, N.L. Saini, A. Bianconi, J.L. Hazemann, Y. Soldo, F.C. Chou, D.C. Johnston, Phys. Rev. B **55**, 9120 (1997).
42. N.L. Saini, A. Lanzara, A. Bianconi, H. Oyanagi, Phys. Rev. B **58**, 11768 (1998).
43. *X-Ray Absorption: Principle, Applications Techniques of EXAFS, SEXAFS and XANES*, edited by R. Prinz, D. Koningsberger (J. Wiley and Sons, New York 1988).
44. A. Lanzara, N.L. Saini, M. Brunelli, F. Natali, A. Bianconi, P.G. Radaelli, S-W. Cheong, Phys. Rev. Lett. **81**, 878 (1998).
45. E.A. Stern, Y. Ma, O. Hanske-Petitpierre, C.E. Bouldin, Phys. Rev. B **46**, 687 (1992).
46. Y.A. Babanov, V.R. Shvetsov, J. Phys. Colloq. France **47**, C8-37 (1986); J. Non Cryst. Sol. **79**, 1 (1986).
47. N.L. Saini, J. Avila, A. Bianconi, A. Lanzara, M.C. Asensio, S. Tajima, G.D. Gu, N. Koshizuka, Phys. Rev. Lett. **79**, 3464 (1997).
48. A. Bianconi, A. Valletta, A. Perali, N.L. Saini, Physica C **296**, 269 (1998); A. Bianconi, European Patent N. 0733271, *High T_c superconductors made by metal heterostuctures at the atomic limit* (priority date 7 Dec 1993), published in European Patent Bulletin 98/22, May 27 1998); `http://www.superstripes.com/`